Published OnlineFirst February 3, 2009; DOI: 10.1158/1535-7163.MCT-08-0707

CNOB/ChrR6, a new prodrug enzyme cancer chemotherapy

Steve H. Thorne,[2] Yoram Barak,[1] Wenchuan Liang,[2] Michael H. Bachmann,[2] Jianghong Rao,[3] Christopher H. Contag,[1,2,3] and A. Matin[1]

[1]Department of Microbiology and Immunology, [2]Department of Pediatrics and Bio-X Program, James H. Clark Center, and [3]Department of Radiology and Molecular Imaging Program, Stanford University School of Medicine, Stanford, California

Abstract

We report the discovery of a new prodrug, 6-chloro-9-nitro-5-oxo-5*H*-benzo(*a*)phenoxazine (CNOB). This prodrug is efficiently activated by ChrR6, the highly active prodrug activating bacterial enzyme we have previously developed. The CNOB/ChrR6 therapy was effective in killing several cancer cell lines *in vitro*. It also efficiently treated tumors in mice with up to 40% complete remission. 9-Amino-6-chloro-5*H*-benzo(*a*)phenoxazine-5-one (MCHB) was the only product of CNOB reduction by ChrR6. MCHB binds DNA; at nonlethal concentration, it causes cell accumulation in the S phase, and at lethal dose, it induces cell surface Annexin V and caspase-3 and caspase-9 activities. Further, MCHB colocalizes with mitochondria and disrupts their electrochemical potential. Thus, killing by CNOB involves MCHB, which likely induces apoptosis through the mitochondrial pathway. An attractive feature of the CNOB/ChrR6 regimen is that its toxic product, MCHB, is fluorescent. This feature proved helpful in *in vitro* studies because simple fluorescence measurements provided information on the kinetics of CNOB activation within the cells, MCHB killing mechanism, its generally efficient bystander effect in cells and cell spheroids, and its biodistribution. The emission wavelength of MCHB also permitted its visualization in live animals, allowing noninvasive qualitative imaging of MCHB in mice and the tumor microenvironment. This feature may simplify exploration of barriers to the penetration of MCHB in tumors and their amelioration. [Mol Cancer Ther 2009;8(2):333–41]

Introduction

Prodrugs are nontoxic in their native state but are converted to toxic products by appropriate enzymes (1–7). Their effectiveness in treating cancer depends either on enzymes that are highly expressed in malignant cells or on foreign activating enzymes that are targeted to tumors. Mitomycin C is an example of the former condition: It is effective because the concentration of the enzyme that activates it, the mammalian NQO1 (also called DT-diaphorase), increases in cancer cells (8), making them more vulnerable than normal cells to its action. In contrast, the effectiveness of 5-aziridinyl-2,4-dinitrobenzamide (CB1954), which is currently in clinical trial for cancer treatment (9), depends on the delivery specifically to tumors of the gene encoding the *Escherichia coli* nitroreductase enzyme, NTR (encoded by *nfsB/nfnB* genes; ref. 5). The latter approach is termed gene-delivered enzyme prodrug therapy (GDEPT); other examples of DEPT therapy are directed delivery of enzymes, catalytic antibodies, and antibody subunits (10, 11).

We previously reported on an improved *E. coli* nitroreductase, ChrR6 (also called Y6), with much greater activity for generating lethal agents from mitomycin C and CB1954 (7). We show here that ChrR6 is highly effective also in activating a new reductive prodrug that we have discovered, 6-chloro-9-nitro-5-oxo-5*H*-benzo(*a*)phenoxazine (CNOB). We were led to a study of this Molecular Probes compound initially because its reduced product, 9-amino-6-chloro-5*H*-benzo(*a*)phenoxazine-5-one (MCHB; Supplementary Fig. S1),[4] is fluorescent at an emission wavelength that can be visualized noninvasively, and because CNOB resembles CB1954 in having a nitro-substituted benzene ring. This raised the possibility that we could indirectly visualize CB1954 reach within animals and tumors by the quenching it might produce of MCHB fluorescence. Indeed, we found that CB1954 competitively inhibited CNOB reduction by our nitroreductase enzymes ChrR (also called YieF) and ChrR6 (7). Subsequent studies, however, showed that CNOB is an effective prodrug in its own right and that it should permit direct noninvasive visualization of its activation. We show that reduction of

Received 7/25/08; revised 10/29/08; accepted 11/19/08;

published OnlineFirst 02/03/2009.

Grant support: U.S. Department of Energy grants DE-FG03-97ER-62490 and DE-FG03-96ER20228, National Cancer Institute grant 1 RO1 CA125074-01A1, and Stanford Office of Technology Licensing grant 1105626 (A. Matin); National Cancer Institute In vivo Molecular Imaging Center at Stanford grant P50 CA114747 (S.H. Thorne and C.H. Contag); and the John A and Cynthia Fry Gunn Research Fund (W. Liang). Y. Barak was supported in part by a Lady Davis postdoctoral fellowship.

The costs of publication of this article were defrayed in part by the payment of page charges. This article must therefore be hereby marked *advertisement* in accordance with 18 U.S.C. Section 1734 solely to indicate this fact.

Note: S.H. Thorne and Y. Barak contributed equally to this work and should be regarded as joint first authors. Current address for S.H. Thorne: Division of Surgical Oncology, Hillman Cancer Center, Suite G12g, 5117 Centre Avenue, University of Pittsburgh, Pittsburgh, PA 15213. Current address for W. Liang: Department of Developmental Biology, Stanford University School of Medicine, Beckman Center, 279 Campus Drive, Stanford, CA 94305-5329.

Requests for reprints: A. Matin, Department of Microbiology and Immunology, Sherman Fairchild Science Building, Stanford University School of Medicine, 299 Campus Drive, Stanford, CA 94305. Phone: 650-725-4745; Fax: 650-725-6757. E-mail: a.matin@stanford.edu

doi:10.1158/1535-7163.MCT-08-0707

[4] Supplementary material for this article is available at Molecular Cancer Therapeutics Online (http://mct.aacrjournals.org/).

Published OnlineFirst February 3, 2009; DOI: 10.1158/1535-7163.MCT-08-0707

CNOB by ChrR6 generates MCHB, which is the agent responsible for cell killing, and present evidence on the probable mechanism of this effect. MCHB fluorescence (excitation 575 nm; emission 625 nm) greatly facilitated examination of the kinetics of CNOB reduction by ChrR6-generating cancer cells and its bystander effect *in vitro*, as well as qualitative visualization of its generation in living mice. CNOB/ChrR6 proved to be an effective treatment of implanted tumors in mice, especially if the distribution of the enzyme within the tumor is improved. The fact that MCHB can be visualized in living mice is likely to facilitate improving its production specifically in tumors and increasing its reach within them.

Materials and Methods

Bacterial Strains, Plasmids, and Cell Lines

Salmonella typhimurium strain SL7838 has been described previously (7, 12). This strain contains deletions in the *aroA* and *sopE* genes, which make it nonvirulent and more specific for targeting tumors. The bacterium was transformed by electroporation (13) with expression plasmids (Supplementary Table S1)[4] encoding the bacterial Lux operon (pCGSL1), green fluorescent protein (GFP; pFVP25.1), and ChrR6 (pET28a$^+$; ChrR6; ref. 7), which is an improved version of the *E. coli* ChrR wild-type nitroreductase with markedly increased capacity for the activation of reductive prodrugs CB1954 and mitomycin C (7). Pure ChrR and ChrR6 were generated as described previously (7). JC (murine mammary cancer) cells were obtained from Cancer Research UK; 4T1 (murine mammary cancer), MCF-7 (human mammary cancer), HeLa (human cervical cancer), HCT 116 (human colorectal cancer), and 293T human embryonic kidney cancer cells were obtained from American Type Culture Collection. Cells were grown as adherent cultures in DMEM supplemented with 10% fetal bovine serum and 1% penicillin and streptomycin (0.5 units and 0.5 μg/mL, respectively; Invitrogen). CNOB/ChrR6 regimen was equally effective against these cell lines; the studies presented here focus on three of them: JC (*in vitro* and *in vivo* killing and visualization), 4T1 (*in vivo* killing, visualization, and MCHB killing mechanism), and HCT 116 (MCHB killing mechanism). Results presented are representative of different cell lines.

In vitro Viability Assays

The effect of converted prodrug on cell lines was measured as described before (7). Prodrug reduction mixtures containing CNOB (Molecular Probes-Invitrogen) and pure ChrR6, 1 mmol/L NADPH, and DMEM added to a final volume of 0.5 mL were allowed to carry out drug reduction at 37°C for 30 min before addition to cancer cells. The extent of drug activation was inferred from the loss of cell viability after 30 min. Cell viability was determined by MTS assay according to the manufacturer's instructions (CellTiter 96AqueousOne, Promega). A_{490} was measured in an ASYS UVM 340 plate reader (Asys Hitech). In control experiments, CNOB was added to cells without ChrR6 and viability was determined by the MTS assay as before.

ChrR6 was also delivered to cancer cells, as specified, from a GDEPT system involving *S. typhimurium* strain SL7838-*chrR6*, with strain SL7838 being used as control. The strains also expressed GFP, which permitted visualization of cell infection. Different multiplicities of infection [MOI; bacterial colony forming units (CFU)/cancer cell] were added to cells in black-walled 96-well plates along with 15 μmol/L CNOB. After 1-h incubation, fluorescence (GFP: excitation 488 nm, emission 525 nm; MCHB: excitation 575 nm, emission 625 nm) was measured using a plate reader with appropriate filters (SpectraMax, Molecular Devices/MDA Analytic Technologies). Cell viability was determined as described above.

Kinetic Constants and Killing Mechanism

To determine enzyme kinetics, 100 μL of 0.1 mol/L Tris-HCl buffer (50 mmol/L; pH 7), 20 μg/mL pure ChrR6, and 100 μmol/L NADPH were mixed. The concentration of CNOB was varied from 0.5 to 2.5 μmol/L and the progress of the reaction was followed by measuring fluorescence at intervals of 1 to 10 min. Kinetic parameters were estimated using Excel plots of linear regression of reciprocals of V_{max} and K_m. Standard curves relating fluorescence and MCHB (ChemBridge) concentrations were generated and used to determine MCHB levels. CNOB reduction product was determined by high-performance liquid chromatography using the following conditions: flow rate, 3 mL/min; detection wavelength, 280 nm (CNOB), 500 nm (MCHB); mobile phase, RP C18, 5 μm; column-packing, Phenomenex Luna 5μ C18(2); dimensions, 250 × 10 mm; injection volume, 100 μL. Gradients of acetonitrile containing 0.1% trifluoroacetyl or trifluoroacetic acid (*TFA*; ''A'') and of water containing 0.1% trifluoroacetyl or trifluoroacetic acid (''B'') were as follows: 0, 3, 28, and 30 min, A: 10% B: 90%; 25 and 28 min, A: 100%, B:0%.

The redox balance method to determine the proportion of electrons used in CNOB reduction and reactive oxygen species (ROS) generation was determined by quantifying the NADPH consumed and H_2O_2 produced during ChrR6-catalyzed CNOB reduction. The former was done spectrophotometrically, and the latter fluorometrically, using the Amplex Red kit (Molecular Probes/Invitrogen), as before (14, 15).

For DNA binding assays, 1 μg of pUC19 plasmid DNA was mixed with 1 μmol/L MCHB or Tris buffer (control) for 10 min. The DNA was then purified by phenol/chloroform extraction, ethanol precipitated, and redissolved in Tris-EDTA buffer. The differently treated DNA samples were run on 1% agaraose in parallel; bands were then cutout from the gel and MCHB fluorescence was read in a plate reader (SpectraMax, Molecular Devices).

To conduct cell cycle assays, nonconfluent cells were treated with 0.1 μmol/L MCHB for 24 h before collection and staining with 7-amino-actinomycin D. Flow cytometry was used to remove doublets, and gates representing G_1, S, and G_2-M phase cells were set. Annexin-phycoerythrin staining was used to examine apoptosis 3 h after MCHB (1 μmol/L) addition to cells using flow cytometry.

Published OnlineFirst February 3, 2009; DOI: 10.1158/1535-7163.MCT-08-0707

For assaying caspase activity, MCHB was added to cancer cells (1 μmol/L) for 1 h, and caspase activities were assayed using Apoalert Caspase assay (Clontech). MCHB-mitochondrial colocalization was determined using Mito-Tracker green FM dye (Molecular Probes). Cells were incubated for 1 h with 1 μmol/L MCHB; 200 nmol/L of MitoTracker green FM was then added, followed by an additional 1-h incubation. Confocal microscopy (TCS SP2 Leica Microsystems) was used to visualize the colocalization of MCHB and the mitochondria. Mitochondrial membrane potential was assayed using the JC Mitochondrial Assay (Molecular Probes) 3 h after addition of MCHB (1 μmol/L).

In vitro Visualization of CNOB Reduction in Live Cells

Cells were grown as adherent cultures and mixed with SL7838 expressing both GFP and ChrR6 at specified MOI values (Results). One hour later, the cells were washed to remove extracellular bacteria, and CNOB was added (15 μmol/L) along with gentamicin (20 μg/mL) to suppress bacterial growth. The conversion of CNOB to fluorescent product (MCHB) and the location of the GFP-expressing bacteria were followed using a confocal microscope (TCS SP2, Leica). Spheroids were formed by growing JC cells on non–tissue-culture-treated plates; transferred to chamber well slides (Lab-Tek, Nunc/Thermo Fisher); and treated with bacteria, CNOB, and gentamicin as before. Prodrug conversion and bacterial GFP were imaged using a two-photon microscope (Carl Zeiss, Inc.).

In vivo Qualitative Visualization of MCHB and Efficacy of CNOB/ChrR6 Tumor Treatment

Immunocompetent BALB/c mice were s.c. implanted with 4T1 cells (1×10^5) expressing luciferase. Tumors were allowed to form for 14 d, at which point they were ~100 mm^3 in size. Animals were then intratumorally injected with 1×10^5 CFU of SL7838 expressing the Lux operon and ChrR6. After 1, 3, and 5 d, they were injected i.v. with 0.1 mg of CNOB (in 100 μL; 3.3 mg/kg) each day (ca. 10 mg total CNOB/kg) or with PBS ($n = 8$ mice/group). (CNOB was initially dissolved in DMSO and then diluted 1:10 in PBS immediately before injection.) MCHB production was qualitatively imaged in living animals using a Maestro system (CRI, Inc.) with dsRed filter sets and spectral unmixing. Imaging of bacterial Lux activity was done using an IVIS100 system (Xenogen/Caliper); imaging of firefly luciferase (Luc)–expressing 4T1 cells was done 5 min after i.p. injection of luciferin (150 μL of 30 mg/mL). The signal generated after luciferin addition (Luc expression) includes the signal due to the bacterial Lux expression; however, because the former was >50-fold greater, the latter was negligible.

Generating 4T1 Cells Transfected to Express ChrR6

In one experimental regimen, the efficacy of CNOB/ChrR6 treatment was determined by initiating tumors with bioluminescent 4T1 cells with constitutive capacity to produce ChrR6. These cells were generated by transposon-mediated gene transfer of human codon optimized *chrR6* gene [encoding humanized ChrR6 (HChrR6) enzyme; GeneScript Corp.] and firefly luciferase (*luc*) in the transposon vector pKT2/BsdR=EGFP-fLuc (pKT2/BGL for short; ref. 16). Briefly, *HchrR6* gene was cloned into the *Sleeping Beauty* transposon, pKT2/UXbG (Supplementary Table S1),[4] using *Hin*dIII/*Apa*I restriction sites, creating pKT2/hU-H*chrR6*-SN. Cells were grown to 90% to 95% confluency in DMEM without antibiotics in a six-well plate. Transposase vector (pUb-SB11; 0.8 μg) and transposon DNA (pKT2/hU-H*chrR*-SN and pKT2/BGL; 7.2 μg) were added to 0.5 mL OptiMem (Invitrogen). In a second vial, 20 μL of Lipofectamine 2000 (Invitrogen) were added to 0.5 mL of OptiMem, and incubation was done at room temperature for 5 min.

The medium was aspirated and cells were washed once with PBS. The above solutions were combined (total of 1 mL/well), added to each well, and incubated for 18 to 24 h. The transfection solution was then aspirated and replaced by regular complete DMEM. Transfection efficiency was monitored by adding 2 to 5 μL of luciferin (30 mg/mL) per well, and imaging done immediately using the IVIS50 system; whereas the untranfected cells expressed no Luc luminescence, the transfected ones showed high expression. Cells were incubated for an additional 48 h and selected with blasticydin and geneticin (Invitrogen; 5 and 2 μg/mL, respectively; these concentrations were predetermined as the minimal killing dose for 4T1 cells). To ensure homogeneity of *HchrR6* expression, cells expressing luciferase were diluted to ~30 cells per 10-mL DMEM, supplemented with the selection antibiotics, and 100-μL aliquots were dispensed into a 96-well plate. This dilution generates a ~30% probability of a well receiving a cell, ensuring that colonies developing in a well originated from a single cell. Tumors from these cells were generated as before.

Tumor burden was measured by caliper measurement at specified times after CNOB treatment. Whole blood counts and the chemistry panel measurements were done by the Stanford Veterinary Service Center. All animal studies were done according to approved Institutional Animal Care and Use Committee and biosafety committee protocols.

Statistical Analyses

Student's t test was done for all statistical analyses, except for the Kaplan-Meier survival curves, for which log-rank tests were used. P values are indicated (significance was assigned at $P < 0.05$).

Results

CNOB Reduction Kinetics and Killing Mechanism

As for mitomycin C and CB1954 (7, 17), pure ChrR6 showed improved kinetics for CNOB reduction with an almost 20- and 10-fold increased V_{max} and K_{cat}/K_m, respectively, over the parent ChrR enzyme (Supplementary Table S2)[4] and was much more active in CNOB-mediated killing of cancer cells than was ChrR (data not shown). CNOB/ChrR6 treatment was as effective in killing cancer cells as treatment with CB1954/ChrR6: Exposure to either regimen (drug concentration, 15 μmol/L) for 1 hour generated >80% killing of murine (4T1, JC) and human

Published OnlineFirst February 3, 2009; DOI: 10.1158/1535-7163.MCT-08-0707

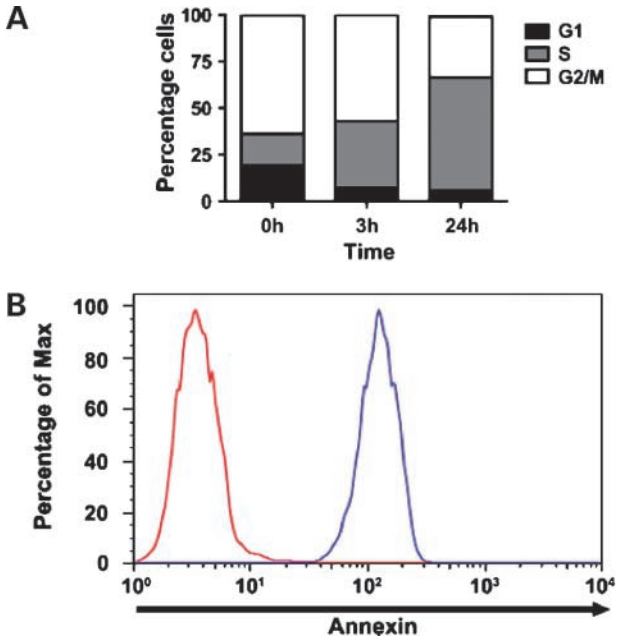

Figure 1. Effect of MCHB on cell cycle and Annexin V. **A,** treatment with MCHB (0.1 μmol/L) results in increasing accumulation of cells in the S phase with time. HCT 116 cells were stained with 7-amino-actinomycin D for cell cycle analysis by flow cytometry. **B,** induction of Annexin V as determined by Annexin V-phycoerythrin staining of the cells: *red graph,* untreated cells; *blue graph,* cells treated with MCHB (1.0 μmol/L, 1 h).

(MCF-7) breast cancer cells as well as of human colorectal (HCT 116), kidney (293T), cervical (HeLa), and other cancer cells (listed in Materials and Methods). Control experiments with CNOB alone were conducted as described in Materials and Methods; these generated no cell killing. (All experiments were conducted in triplicate; $P < 0.05$.).

High-performance liquid chromatography was used to characterize the products of CNOB reduction by ChrR6. The only compound besides CNOB found in a reaction mixture containing pure ChrR6, NADPH, and CNOB was MCHB (data not shown). Generation of MCHB from CNOB requires a two-electron reduction, but the nitro group present in CNOB has a predilection for accepting one electron, which would result in the formation of CNOB nitro-radical anions (Supplementary Fig. S1).[4] These are short lived and cannot be detected by high-performance liquid chromatography analysis. As these anions have a redox potential lower than the oxygen couple, they redox cycle. In this process, the one-electron–reduced CNOB anion would be rapidly oxidized back to CNOB, giving its electron to dioxygen, resulting in ROS generation. Due to its repetitive nature, this process would produce large quantities of ROS. To detect whether redox cycling occurs during CNOB reduction by ChrR6, we used our redox balance method (14, 15). This entailed quantification of the reductant (NADPH) electrons partitioned between MCHB and ROS generation. Little ROS production was found, with >80% of NADPH electrons being used in CNOB reduction. Thus, there was minimal or no single-electron reduction and redox cycling of the prodrug. (Note that some ROS can result from disproportionation of MCHB; ref. 18.) The results strongly suggest that MCHB is the sole product of CNOB reduction by ChrR6.

What might be the mechanism of MCHB killing of cancer cells? In addressing this question, we were guided by the example of CB1954 because CNOB and CB1954 are both nitro-prodrugs and, as stated above, kill mammalian cells with equal efficiency when activated by ChrR6. The reduction product of CB1954 kills cells through DNA intercalation (19). The CNOB reduction product, MCHB, did indeed bind DNA (Supplementary Fig. S2)[4] and, as is typical of DNA intercalating agents, caused HCT 116 cell accumulation in the S phase at nonlethal concentration 0.1 μmol/L (Fig. 1A). At lethal dose (1.0 μmol/L), MCHB was apoptotic as indicated by rapid increases in cell-surface Annexin V (Fig. 1B) and caspase-3 (Fig. 2A) activity. Microscopic evidence pointed to focal localization of MCHB mainly within the cytoplasm (Fig. 3C;

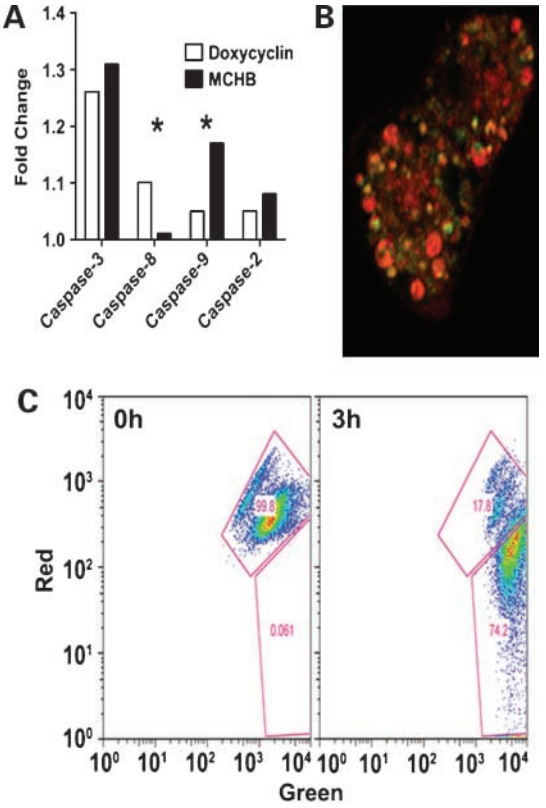

Figure 2. Effect of MCHB on caspases and mitochondria. **A,** induction of caspase activities on treatment of HCT 116 with 1 μmol/L MCHB, relative to untreated cells or doxycycline (known to induce apoptosis through activation of caspase-8 and caspase-3; $*P < 0.05$). **B,** colocalization of MCHB with mitochondria of HCT 116 (stained with MitoTracker green FM) as visualized by confocal microscopy (×60 magnification). **C,** MCHB effect on mitochondrial membrane potential: JC-1 staining of MCHB treated HCT 116 cells. Increase in green staining (*X-axis*) and decrease in red staining (*Y-axis*) indicate mitochondrial depolarization.

Published OnlineFirst February 3, 2009; DOI: 10.1158/1535-7163.MCT-08-0707

Supplementary Fig. S3),[4] raising the possibility that it was taken up by mitochondria and bound to mitochondrial DNA. When the latter were stained with MitoTracker green FM, colocalization of MCHB and mitochondria was seen (Fig. 2B). MCHB also caused rapid disruption of mitochondrial membrane potential, as indicated by cell population shift toward the ''green'' axis (Fig. 2C). Furthermore, MCHB increased caspase-9 activity (Fig. 2A), indicative of apoptosis initiated through the intrinsic mitochondrial pathway and cytochrome *c* release. The results suggest that MCHB kills the cells by intercalating with mitochondrial DNA and causing apoptosis involving the mitochondrial pathway. Treatment with doxycycline served as control for this experiment. This drug induces apoptosis through caspase-3/8 activation; the expected results were seen (Fig. 2A). The reason for the apparent MCHB preference for mitochondria remains to be determined.

Relationship between Reduced CNOB Fluorescence and Cell Killing *In vitro*

We first determined correlation between MCHB fluorescence and its killing capacity. In the range of 100 to 1,000 nmol/L (which is within linear relationship between MCHB concentration and its fluorescence), MCHB fluorescence intensity was directly proportional to its cell killing activity. Thus, 100, 700, and 1,000 nmol/L MCHB caused 3%, 38%, and 65% cell killing, respectively, of JC, MCF-7, and 4T1 cells after 24-hour incubation. Correlation between fluorescence and cell killing was seen also when the SL7838-*chrR6* GDEPT system was used to generate MCHB from CNOB in attached JC cells. Increasing doses of GFP-producing SL7838-*chrR6* bacteria resulted in a progressive increase in MCHB generation, as detected by GFP and MCHB fluorescence intensities, respectively (Fig. 3A). The increase in MCHB fluorescence generated increasing cell killing (Fig. 3A and B). In contrast, equivalent levels of infection with SL7838 (not encoding ChrR6), used as control, produced little MCHB and were much less lethal: >10-fold fewer SL7838-*chrR6* bacteria were required to kill 50% of the cell layer compared with SL7838 not expressing this enzyme (Fig. 3A and B). SL7838 by itself also generated cancer cell lethality, especially at high doses (Fig. 3B), which is consistent with previous findings (12, 20).

Visualization of CNOB Reduction Kinetics and Bystander Effect *In vitro*

The fluorescence of MCHB afforded a facile means to examine the *in vitro* kinetics of CNOB reduction and the bystander effect of the CNOB/ChrR6 regimen. Bystander effect refers to the spread of the activated drug from cells capable of producing it to the neighboring cells lacking this capacity; it is critical to the efficacy of any DEPT therapy because no DEPT approach can transform all the cancer cells in a tumor. The MCHB fluorescent signal in attached JC cells infected with GFP-expressing SL7838-*chrR6* bacteria was detectable as early as 10 minutes after CNOB (15 μmol/L) addition (Fig. 4A) and increased in intensity with time, reaching a steady state in some 20 to 30 minutes. Quantification of CNOB conversion to MCHB in a fluorescence plate reader in an equivalent experiment gave

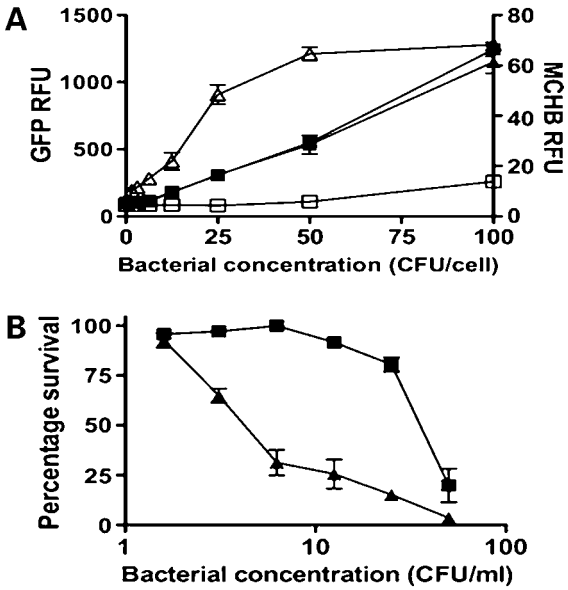

Figure 3. Correlation between MCHB production from CNOB and JC cell killing. The *in vitro* GDEPT system involving different doses of GFP-expressing SL7838-*chrR6* or SL7838 (control) bacteria was used to infect the JC cells exposed to CNOB. Relative fluorescence units (*RFU*) of GFP (indicative of the extent of cell infection by the bacteria) and MCHB [indicative of the extent of CNOB reduction (**A**) and cell killing (**B**)] were measured as described in Materials and Methods. **A,** ▲ and ■, JC cell infection indicated by GFP levels by SL7838-*chrR6* and SL7838, respectively (note that cancer cells were infected by both strains to the same extent); △ and □, MCHB generation by cells infected with SL7838-*chrR6* and SL7838, respectively. **B,** ▲ and ■, killing of SL7838-*chrR6*– and SL7838-infected cells, respectively. Note that despite equivalent degree of infection by the two bacterial strains, SL7838-*chrR6*–infected cells exhibit markedly more MCHB generation and cell killing.

similar results (Fig. 4B). Note that when uninfected cancer cells were treated with CNOB (Fig. 4A, ''C-30''), or when infected cells were not exposed to CNOB (Fig. 4B), no fluorescence was generated. Image ''GFP-30'' shows GFP fluorescence of bacteria and their location in a parallel monolayer that did not receive CNOB. Thus, the indigenous nitroreductases of these cells did not activate CNOB, and the red fluorescence seen in Fig. 4 was due to MCHB.

To examine the bystander effect, we repeated the above experiment at a MOI of 1 CFU/cell, resulting in ~20% of cancer cells becoming infected. It is evident (Fig. 4C) that by 30 minutes after CNOB addition, the red signal of MCHB is present not only in cells infected with the bacteria (green and yellow spots; Fig. 4C) but also in the uninfected ones. We also examined this effect in three-dimensional tissue culture cell spheroids because the latter are more representative of conditions within solid tumors than cell monolayers (21). There was extensive MCHB presence in the spheroids including in areas away from the bacteria (green/yellow), as visualized by two-photon microscopy (Fig. 4D). However, zones are seen within them where the red fluorescence is absent (Fig. 4D; Supplementary Fig. S4).[4] This may be because of penetration barriers to CNOB and/or MCHB within the spheroids.

Published OnlineFirst February 3, 2009; DOI: 10.1158/1535-7163.MCT-08-0707

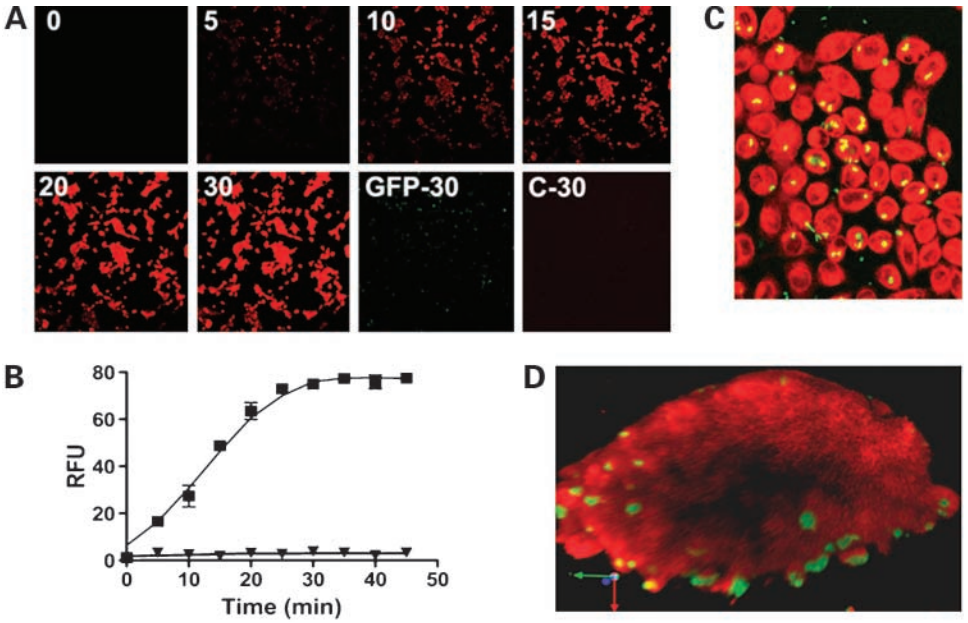

Figure 4. *In vitro* imaging of MCHB within JC cancer cells. **A,** kinetics of CNOB reduction as visualized by the generation of MCHB fluorescence in JC cells infected with GFP-expressing SL7838-*chrR6* at MOI of 10 per cell. Cells were imaged by confocal microscopy at the indicated times (in minutes) after CNOB addition (×4 magnification). See Materials and Methods for details. *GFP-30,* GFP fluorescence from bacterial cells at 30 min from monolayers to which no CNOB was added. *C-30,* a control plate of cells treated with CNOB, but not SL7838-*chrR6*, imaged 30 min after the addition of CNOB. **B,** an equivalent experiment was run and CNOB conversion to MCHB was quantified at the indicated times following CNOB addition in a fluorescence plate reader for cells with or without CNOB addition (■ and ▲, respectively). **C,** the experiment in Fig. 3A was repeated using a MOI of 1.0 CFU/cell, resulting in ~20% of cells becoming infected. The representative image shown was taken 30 min after CNOB addition (×20 magnification). **D,** JC cells were used to form multicellular tumor spheroids. SL7838-*chrR6* expressing GFP was added at a MOI of ~1,000 CFU/spheroid and incubated for 30 min to permit infection. Images were taken by two-photon microscope 1 h after CNOB addition. Z-stack images were reconstructed into a three-dimensional model using Velocity software and snapshots were taken from different angles. Note that the image represents a cross section through the center of the spheroid and 95-μm depth.

Visualization of CNOB Reduction *In vivo*

The emission wavelength of MCHB (625 nm) is such that it raises the possibility of its visualization by noninvasive methods in live animals. To qualitatively explore this possibility, we established tumors (expressing Luc) in mice followed by intratumoral administration of Lux-expressing SL7838-*chrR6* and i.v. injection of CNOB (3.3 mg/kg) 24 hours later. Noninvasive imaging (see Materials and Methods) of living animals revealed the presence of the bacteria (*blue*; Lux luminescence) and MCHB fluorescence (*red*) in the infected tumors only (*blue*; Lux and Luc luminescence; Fig. 5). Control tumors not infected with the bacteria (Luc luminescence only) do not show the MCHB fluorescence; some fluorescence in the kidneys of these mice can, however, be detected.

We found that CNOB/SL7838-*chrR6*–treated mice displayed easily detectable levels of MCHB (as measured by its fluorescence) in their blood in contrast to the control animals injected with CNOB alone (Fig. 5B). To determine if the MCHB in the blood caused hematopoietic toxicity, whole blood counts were done. Apart from the expected increase in WBC due to bacterial infection, no adverse effects were seen (data not shown). This raises the possibility that MCHB secreted into the blood might prove useful in assessing the efficacy of CNOB delivery and activation *in vivo*.

Solid tumors constitute a complex microenvironment (21), and we wondered if MCHB fluorescence would permit the visualization of its distribution within this environment. This was attempted, again only qualitatively, in SL7838-*chrR6*– and CNOB-inoculated tumors (intratumorally and i.v., respectively, as above) in living mice using intravital microscopy. Angiosense 680 was also injected i.v. to visualize the vasculature. The CNOB signal was first seen at 10 minutes postinoculation (data not shown). At 60 minutes (Fig. 5C), the red fluorescence was quite marked and was seen primarily in zones of maximal vascularization (*white*) rather than in association with the ChrR6 producing bacteria (*green*).

Effect of CNOB/ChrR6 Treatment on Mouse Tumors

For *in vivo* studies of CNOB/ChrR6 therapy, 4T1 cells were used to initiate the tumors. These form especially aggressive tumors, so the efficacy of the treatment could be tested in an extreme situation. (Note that, as stated in Materials and Methods, *in vitro* 4T1 cells respond to CNOB/ChrR6 treatment in the same way as the JC cells; Fig. 4.) To ensure uniform ChrR6 generation within the tumors in these exploratory *in vivo* studies of the efficacy of the therapy, we made use of 4T1 cells transfected to constitutively express HChrR6 to initiate s.c. tumors in immunocompetent BALB/c mice. Two CNOB concentrations,

Published OnlineFirst February 3, 2009; DOI: 10.1158/1535-7163.MCT-08-0707

3.3 mg/kg (single dose) or 10 mg/kg (spaced in three doses–see Materials and Methods), were used and administered i.v. Whereas the control mice injected with PBS were all dead within 25 days, at 3.3 mg/kg, 60% mice were still alive by day 60 after CNOB injection (Fig. 6A); at 10 mg/kg, there was 40% complete remission up to 150 days ($P = 0.0012$).

To test the efficacy of the treatment in a clinically more relevant setting, we induced tumors in mice using untransfected 4T1 cells and delivered the enzyme using SL7838-*chrR6* intratumoral GDEPT system; CNOB (10 mg/kg) was injected i.v. As expected from previous findings (7, 12, 20) and the data of Fig. 3B, the bacteria alone slightly increased mice survival, but this was enhanced in mice given CNOB/SL7838-*chrR6* (Fig. 6B; $P = 0.0012$): Animals receiving the bacteria alone were all dead by day 35, but in the regimen involving CNOB administration, 10% were still alive on day 60. It is clear, however, that the treatment in this setting is less effective than that of Fig. 6A, suggesting, in agreement with the data of Fig. 5C, that in this DEPT system, even at the higher CNOB concentration, enzyme and/or the drug/MCHB fails to effectively disseminate in the tumor.

Blood chemistry panel values showed no major toxicity up to a CNOB concentration of 20 mg/kg (Supplementary Table S3).[4] Some slight muscular damage may be indicated by marginal elevation of markers such as creatine phosphokinase, and that of kidneys by those of blood urea nitrogen, calcium, and phosphate. The latter would seem to be consistent with the slight activation of the drug in kidneys of mice not given ChrR6-encoding bacteria (Fig. 5A, *bottom*). However, because the effects are minor, CNOB would seem to be largely nontoxic.

MCHB Fluorescence and Determination of Its Biodistribution

Can MCHB biodistribution be determined by simple fluorescence measurements? To address this question, we repeated the experiment of Fig. 5, except that SL7838-*chrR6* bacteria were administered i.v. Imaging showed that, as expected (12), this resulted in bacterial colonization of organs besides the tumor. The red fluorescence was seen not only in the tumor but also in other organs (data not shown). Postmortem determination of MCHB fluorescence intensity in different organs and use of a standard curve made it possible to measure the quantity of MCHB (Supplementary Fig. S5);[4] most was still generated within the tumor (for which SL7838 has a predilection) but it was also seen in other organs.

Discussion

We show that the new CNOB/ChrR6 therapy is highly effective in killing different cancer cells lines *in vitro*. To determine if the therapy is useful in treating cancer in a mouse model, we first implanted mice with s.c. tumors that endogenously (and constitutively) generated a humanized form of ChrR6 (HChrR6) to ensure uniform generation of the enzyme within the tumor. I.v. administered CNOB in this situation generated beneficial results, especially at 10 mg/kg dose, which resulted in some 40% mice showing complete remission. (At this concentration, the expected peak tissue drug concentration is approximating 14 μmol/L.) We then used a clinically more relevant setting in which mice were implanted with nontransfected 4T1 tumors not generating their own ChrR6 and delivered the enzyme by an intratumorally administered SL7838-*chrR6* GDEPT system. Again, beneficial results were seen, although they were less

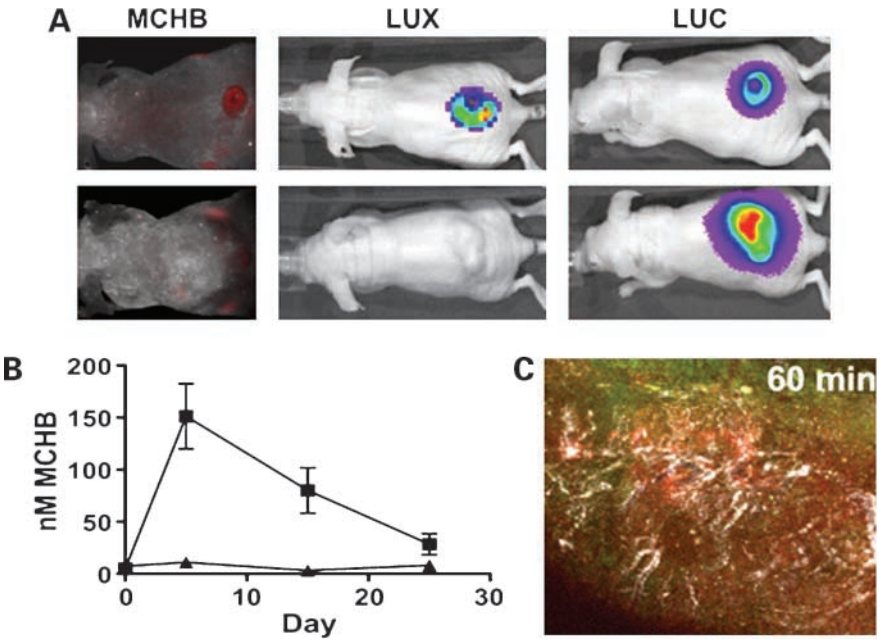

Figure 5. **A,** visualization of MCHB generation (*red fluorescence*) in JC implanted tumors in living mice by noninvasive imaging at 6 h after CNOB administration. Lux-expressing SL7838-*chrR6* bacteria were injected intratumorally, and CNOB (*top*, mouse only) i.v., 24 h later. Luc and Lux luminescence represent the location of tumors and the bacteria, respectively. (The Luc signal includes Lux, but because the former was >50-fold greater, the latter is negligible; see Materials and Methods.) Note the absence of red fluorescence in tumors of mice not injected with bacteria but given CNOB (*bottom*). **B,** MCHB levels (quantified from fluorescence measurements) in blood samples collected by bleeding mice at indicated time points: ■, CNOB/SL7838-*chrR6*–treated mice; △, CNOB-only–treated mice. **C,** qualitative visualization of MCHB generation in tumor in a living mouse (intravital microscopy) in relation to vasculature (*white*) and the *ChrR6*-generating bacteria (*green*). CNOB and SL7838-*chrR6* were administered as above.

Published OnlineFirst February 3, 2009; DOI: 10.1158/1535-7163.MCT-08-0707

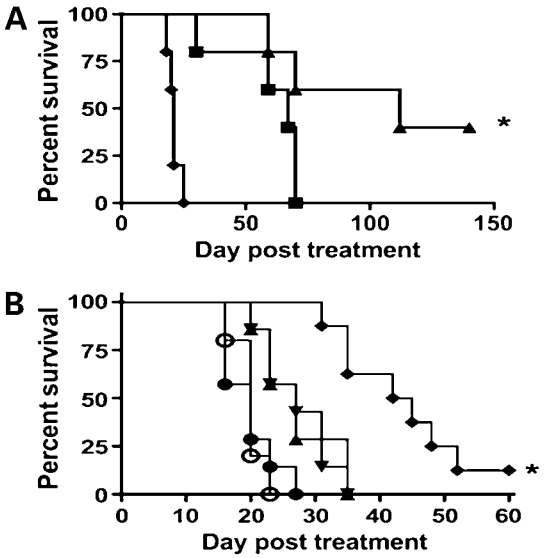

Figure 6. *In vivo* efficacy of CNOB/ChrR6 treatment. **A,** survival (Kaplan-Meier) curves of mice implanted with 4T1 tumors (50 – 100 mm^3) endogenously expressing HChrR6 and treated with PBS (♦), 3.3 mg/kg CNOB (■), or 10 mg/kg CNOB (▲); $n = 5$ animals per group. *, $P = 0.0018$. **B,** survival (Kaplan-Meier) curves of mice implanted with nontransfected 4T1 tumors (50 – 100 mm^3) not expressing ChrR6 and treated with PBS (○), CNOB alone (●), SL7838-*chrR6* alone (▲), SL7838 and CNOB (▼), or SL7838-*chrR6* and CNOB 10 mg/kg (♦); $n = 8$ animals per group. $P = 0.0012$, SL7838 and CNOB compared with SL7838-*chrR6* and CNOB. Bacteria (1×10^5 CFU) were administered via intratumoral injection on day 0; CNOB (3.3 mg/kg each time) was given on days 1, 3, and 5 via i.v. injection. *, $P < 0.05$.

impressive. Thus, whereas on day 60 at 10 mg/kg CNOB, only 10% mice survived in the GPEPT regimen, 60% survived in that involving HChrR6, indicating impediments to the reach of one or more components of the therapy within the tumors in the former regimen. That there may be barriers to the penetration of MCHB is suggested also by cell spheroid (Fig. 4D) and tumor microenvironment imaging (Fig. 5C) results.

This new therapy has certain attractive features. Like CB1954, CNOB most likely kills by intercalating DNA. Thus, like the former, it will target both growing and nongrowing cells, which is advantageous because most cells in solid tumors remain quiescent. In addition, like CB1954, it was not activated by indigenous nitroreductases of several cancer cells. This seems to be the case also in live mice, as indicated by the absence, by and large, of MCHB generation and significant toxicity in mice given CNOB without ChrR6 (Fig. 5A and B; Supplementary Table S3).[4] CNOB, like CB1954, thus holds the promise of affording a generally side effect–free cancer therapy on successful specific GDEPT targeting of ChrR6 to tumors. However, the most attractive feature of CNOB/ChrR6 therapy may turn out to be the fact that its killing agent, MCHB, unlike that of CB1954 [m5-(aziridin-1-yl)-4 hydroxylamino-2-nitrobenzamide], is fluorescent, and its noninvasive visualization in live animals can simplify studies aimed at improving the efficacy of this therapy.

MCHB fluorescence was helpful in *in vitro* as well as *in vivo* studies. The kinetics of CNOB activation within the cells, the MCHB killing mechanism, and its bystander effect including the possibility of barriers to its penetration within the cell spheroids, as well as its biodistribution, were determined by simple fluorescence measurements *in vitro*. Similarly, although only qualitative, MCHB visualization in living mice by noninvasive imaging afforded a facile means of determining the locus of CNOB reduction, including within the tumor microenvironment. This feature is likely to prove valuable in more detailed studies on MCHB generation within solid tumors because, unlike most other drugs, this might be determined in real time without the need of sacrificing the experimental animals.

Real-time imaging of MCHB within the implanted tumors, along with secondary labels such as those against necrotic and hypoxic regions, the vasculature, and the tumor matrix material, can reveal the nature of the impediments to activated drug penetration of tumors. Countermeasures might then be investigated, and because their effects can be visualized noninvasively, several treatments may be tested in the same animal model. We are currently studying these aspects as well as methods for quantitative imaging of MCHB *in vivo*, detailed pharmacokinetics of the CNOB/ChrR6 therapy, further improvement in CNOB activating enzyme (17, 22), and appropriate GDEPT methods (11, 23, 24) to improve this treatment regimen and determine its suitability of for translation to the clinic.

Disclosure of Potential Conflicts of Interest

No potential conflicts of interest were disclosed.

Acknowledgments

We thank Dr. B. Efron for help with statistical analysis, Dr. David Chu for help with blood chemistry panel analysis, and Dr. Michael Benoit for help with the preparation of the manuscript.

References

1. Patterson AV, Saunders MP, Greco O. Prodrugs in genetic chemoradiotherapy. Curr Pharm Des 2003;9:2131 – 54.

2. Dachs GU, Tupper J, Tozer GM. From bench to bedside for gene-directed enzyme prodrug therapy of cancer. Anticancer drugs 2005;16:349 – 59.

3. Denny WA. Nitroreductase-based GDEPT. Curr Pharm Des 2005;8:1349 – 61.

4. Brown JM, Wilson WR. Exploiting tumour hypoxia in cancer treatment. Nat Rev Cancer 2004;4:437 – 47.

5. Knox RJ, Chen S. Quinone reductase-mediated nitro-reduction: clinical applications. In: Sies H, Packer L, editors. Methods in enzymology. Amsterdam: Elsevier 2004;382:437 – 221.

6. Rooseboom M, Commandeur JN, Vermeulen NP. Enzyme-catalyzed activation of anticancer prodrugs. Pharmacol Rev 2004;56:53 – 102.

7. Barak Y, Thorne SH, Ackerley DF, Lynch SV, Contag CH, Matin A. New enzyme for reductive cancer chemotherapy, YieF, its improvement by directed evolution. Mol Cancer Ther 2006;5:97 – 103.

8. Seow HA, Penketh PG, Bauman RP, Sartorelli AC. Bioactivation and resistance to mitomycin C. In: Sies H, Packer L, editors. Methods in enzymology. Amsterdam: Elsevier 2004;382:221 – 33.

Published OnlineFirst February 3, 2009; DOI: 10.1158/1535-7163.MCT-08-0707

9. Chung-Faye GD, Palmer D, Anderson J, et al. Virus-directed, enzyme prodrug therapy with nitroimidazole reductase: a phase I and pharmacokinetic study of its prodrug, CB1954. Clin Cancer Res 2001; 7:2662 – 8.

10. Bagshawe KD. Antibody-directed enzyme prodrug therapy (ADEPT) for cancer. Exp Rev Anticancer Ther 2006;6:1421 – 31.

11. Hood JD, Bednarski M, Frausto R, et al. Nanoparticle-mediated gene delivery to tumour neovasculature. Science 2002;296:2404 – 07.

12. Thorne SH. Strategies to achieve systemic delivery of therapeutic cells and microbes to tumors. Expert Opin Biol Ther 2007;7:41 – 51.

13. O'Callaghan D, Charbit A, High efficiency transformation of *Salmonella typhimurium* and *Salmonella typhi* by electroporation. Mol Gen Genet 1990;223:156 – 8.

14. Ackerley DF, Gonzalez CF, Park CH, Blake R II, Keyhan M, Matin A. Chromate-reducing properties of soluble flavoproteins from *Pseudomonas putida* and *Escherichia coli*. Appl Environ Microbiol 2004;70:873 – 82.

15. Gonzalez CF, Ackerley DF, Lynch SV, Matin A. ChrR, a soluble quinone reductase of *Pseudomonas putida* that defends against H2O2. J Biol Chem 2005;280:22590 – 5.

16. Wilber A, Frandsen JL, Geurts JL, Largaespada DA, Hackett PB, McIvor RS. RNA as a source of transposase for Sleeping Beauty-mediated gene insertion and expression in somatic cells and tissues. Mol Ther 2006; 13:625 – 30.

17. Barak Y, Nov Y, Ackerley DF, Matin A. Enzyme improvement in the absence of structural knowledge—a novel statistical approach. ISME J 2008;2:171 – 9.

18. Cadenas E. Antioxidant and prooxidant functions of DT-diaphorase in quinone metabolism. Biochem Pharmacol 1995;49:127 – 40.

19. Knox RJ, Friedlos F, Jarman M, Roberts JJ. A new cytotoxic, DNA interstrand crosslinking agent, 5-(aziridin-1-yl)-4-hydroxylamino-2-nitrobenzamide, is formed from 5-(aziridin-1-yl)-2,4-dinitrobenzamide (CB1954) by a nitroreductase enzyme in Walker carcinoma cells. Biochem Pharmacol 1988;37:4661 – 9.

20. Zhao M, Geller J, Ma H, Yang M, Penman S, Hoffman RM. Monotherapy with a tumor-targeting mutant of *Salmonella typhimurium* cures orthotopic metastatic mouse models of human prostate cancer. Proc Natl Acad Sci U S A 2007;104:10170 – 4.

21. Minchinton AI, Tannock IF. Drug penetration in solid tumours. Nat Rev 2006;6:583 – 92.

22. Barak Y, Ackerley DF, Dodge CJ, et al. Analysis of novel soluble chromate and uranyl reductases and generation of an improved enzyme by directed evolution. Appl Environ Microbiol 2006;72:7074 – 82.

23. Schepelmann S, Springer CJ. Viral vectors for gene-directed enzyme prodrug therapy. Curr Gene Ther 2006;6:647 – 70.

24. Thorne SH, Negrin RS, Contag CH. Synergistic antitumor effects of immune cell-viral biotherapy. Science 2006;311:1780 – 4.

Published OnlineFirst February 3, 2009; DOI: 10.1158/1535-7163.MCT-08-0707

Molecular Cancer Therapeutics

CNOB/ChrR6, a new prodrug enzyme cancer chemotherapy

Steve H. Thorne, Yoram Barak, Wenchuan Liang, et al.

Mol Cancer Ther 2009;8:333-341. Published OnlineFirst February 3, 2009.